# Final Project Overview

## Melting fat: Modeling the Effects of RFAL using the Invasix BodyTite™ system

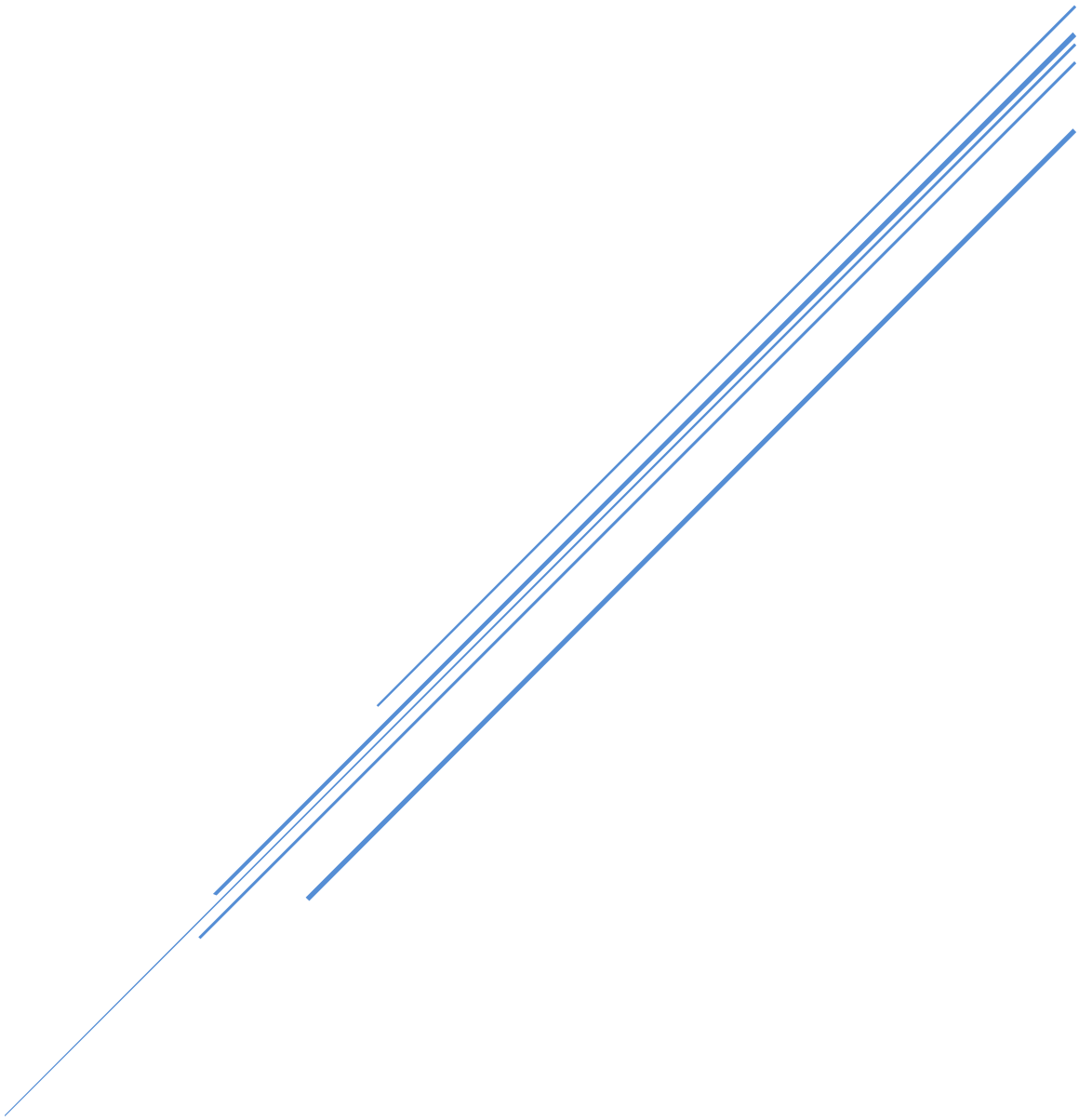

BEE 4530 Computer-Aided Engineering

*Professor Ashim Datta & Teaching Assistant Alex Warning*

**Ashley Fung | Kevin Hua | Malavika Nadig | Gary Wan**

## ABSTRACT

Radio-Frequency Assisted Liposuction (RFAL) is a recent technique that shows promise compared to traditional procedures in terms of safety, recovery times, and results. Currently, however, there lacks an accurate computational model that can be used by researchers to study the efficacy of this technology with optimal parameters. Here we focus on the use of a novel RFAL device (the Invasix BodyTite™) that consists of a RF-emitting, fat-aspirating probe and a grounding sensor. A 3D COMSOL model was implemented with the bio-heat equation coupled with a joule heating mechanism in order to simulate the temperature and fat aspiration profiles, allowing analysis of varying levels of output power and probe velocity. The model had mean dimensions of skin, adipose, and muscle thickness proportional to measurements of arms and thighs found in literature, while the material properties were collected as statistical mean from a compilation of online databases and literature sources. Verification was conducted throughout each step of the design process through temperature and heat source graphs, and a mesh convergence was reached at a quality of higher than 30,000 elements. The cumulative fat aspiration is calculated with a volume integration of nodes that reach above the fat melting temperature of 316 K. The total fat volumes extrapolated from our model, within the devices range of power, are compliant with clinically observed results from literature. Furthermore, a sensitivity analysis of key fat parameters showed density, heat capacity, and thermal conductivity to have the largest effect on cumulative fat aspiration. To reach the original objective of assisting researchers with a computational mode, an optimization of probe velocity to cumulative fat aspiration was conducted. The optimal probe velocity for maximum rate of fat aspiration was found to be 3 cm/s.

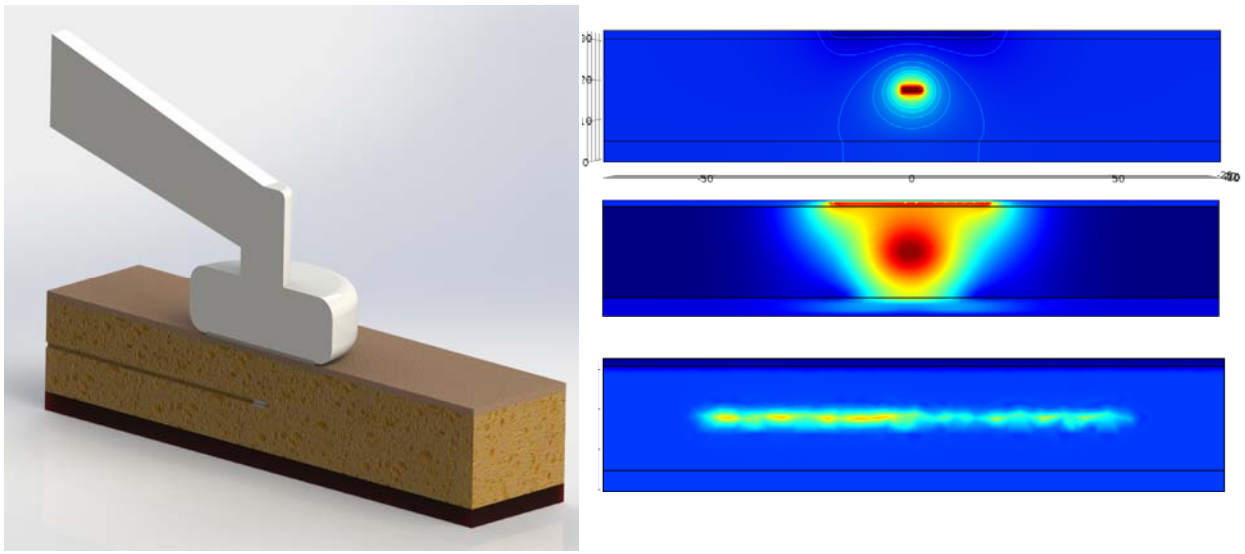

# TABLE OF CONTENTS

## LIST OF FIGURES



## LIST OF TABLES

# I. EXECUTIVE SUMMARY

The main incentive behind our research in this Radio-Frequency Assisted Liposuction (RFAL) system was to computationally solve the surgical situation as a mathematical model governed by input parameters; the resulting model then has the prospect to be used in medical situations to help clinicians make an informed decision before the procedure.

Our research draws on the ability of BodyTite™ (*Invasix, Israel*) to deliver effective treatment based on relevant clinical data. Prior literature describes that the technique relies heavily on the parameters influenced both by the doctor's methodology and the unique needs of the patient. In practice, the RFAL system will be implemented by a surgeon based on individual experiential knowledge of how long and what treatment regions to cover. However, a mathematical model that suggests an optimal power output and treatment method based on the patient's data, such as body fat thickness and skin thickness, complements the surgeon's procedure.

The model we propose suggests an optimal probe speed of the RFAL system to deliver maximum rate of fat aspiration and minimum heating of the skin for individual surgeons to consider. We designed our model to approximate the clinical procedure as closely as possible, and concluded that discretization error is at a minimum by reaching a mesh convergence of our model. Furthermore, we validated our model by extrapolating a moving probe fat volume aspiration and comparing it to experimental data—within the range of RFAL output powers, our fat volume aspiration matched the clinical data. We also performed sensitivity analysis and found that fat parameters including density, heat capacity, and thermal conductivity to be critical factors. In order to reach our design goals of providing recommendation to researchers, we found an optimal probe velocity to reach the maximal fat volume aspiration rate. Based on the practical implications of this model, we would recommend a future design of the BodyTite™ user interface that displays the current velocity of the probe the surgeon is operating.

# II. INTRODUCTION

Radiofrequency-assisted liposuction (RFAL) stands out among recently developed energy-assisted liposuction techniques due to its ability to maintain uniform heating and achieve significant skin tightening. The current standard for RFAL involves the use of Invasix's BodyTite, a device comprised of two electrodes; the internal electrode is inserted through the epidermis and into the subcutaneous fat, while the external electrode rests on the skin's surface. The internal electrode simultaneously aspirates and delivers radiofrequency energy to heat surrounding adipose tissue, increasing the speed and efficiency of a liposuction procedure.

Before the development of energy-assisted procedures, traditional-suction assisted liposuction was the most conventional method. Traditional suction-assisted liposuction (SAL) involves a small cannula used to avulse fat from the skin using a mechanical disruption of adipose tissue. Induced by a negative pressure, the suction cannula can then use a vacuum to aspirate small clusters of fat. This method poses a number of shortcomings; it requires a significant amount of time, has not been effective in skin contraction, typically puts the patient through a high level of discomfort, and poses a risk for complications, including embolisms, skin damage, and excessive fluid loss **[1]**.

Although ranked as the number four most commonly performed aesthetic surgical procedure in 2013, traditional liposuction procedures in the United States have experienced a 44% decrease in number of surgeries since 2000 **[2]**. Patients and doctors are now seeking less invasive, safer methods for performing liposuction that will achieve better results while minimizing scarring. Among these are energy-assisted liposuction techniques, such as ultrasound-assisted (UAL) and laser-assisted (LAL), and the most novel approach, radiofrequency-assisted liposuction (RFAL).

Distinctive features of the BodyTite device include the ability to control power output, threshold temperature, and distance between the external and internal probes. The power output ranges anywhere from 20-75 W allowing physicians to adjust the value based on anatomical location and tissue depth. Threshold skin temperature indicates the temperature at which radiofrequency energy will shut off if detected by the external electrode. The device continually provides temperature feedback, creating a reliable safety measure **[3]**.

Studies have shown that RFAL has been successful in reducing treatment time, inducing significant skin contraction, and executing effective lipolysis. A mathematical model of RFAL technology allows for valuable studies of how different input parameters such as fat material properties, output power, and probe velocity affect the overall surgery.

## III. PROBLEM STATEMENT

There lacks a clinically accurate computational model for radiofrequency assisted liposuction that can be used by researchers to determine the efficacy of the procedure and potential safety hazards associated with varying levels of power and probe velocity. Having such a model allows for researchers to make more informed design decisions pertaining to power output and probe velocity.

## IV. DESIGN OBJECTIVES

Physicians and researchers have shown that at a threshold temperature of 38°C and a power output of 45W for a tissue thickness of 25 mm, RFAL has been successful. We plan to use COMSOL to model radiofrequency-assisted liposuction under these conditions in order to further investigate the design of the procedure and determine the optimal speed of the device. By modeling the procedure under static and dynamic conditions of the probe, we will determine the optimal speed needed to maximize the rate of fat aspiration.

## V. TRANSITION TO MODEL SCHEMATIC

The model schematic is based on the original BodyTite device when inserted into an abdominal, subcutaneous fat layer, as shown below during both heating and fat aspiration (Figure 1). The main components of the actual device are the probe tip inserted into the subcutaneous fat layer—serving as both the source of the radiofrequency field and as a cannula that aspirates the melted fat (Figure 1c)—and the circular, external sensor resting on top of the skin, serving to ground the radiofrequency field.

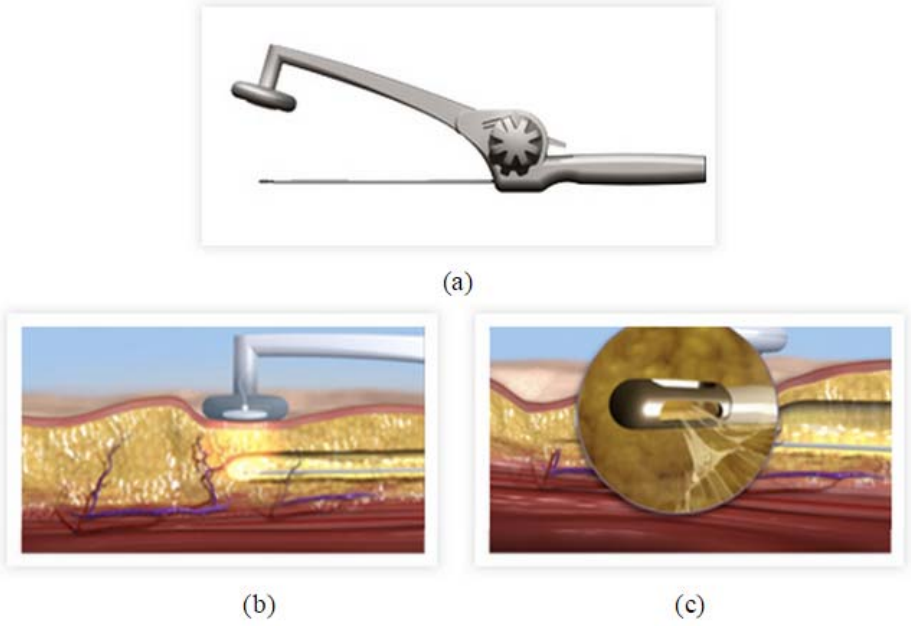


**Figure 1. Original BodyTite Images (obtained from Invasix)**
(a) An overall view of the Invasix device shows how the device can be adjusted to accommodate varying depths of fat. (b) The device functions with two electrodes, one externally resting on the skin and one internally used to apply radiofrequency heat. (c) The internal cannula is capable of simultaneously applying heat and aspirating melted fat.

Representative models were made in conventional software (Figure 2) to help visualize the necessary simplified transition from the complex clinical situation—notice that the layers of skin, fat, and muscle are uniform in geometry. The actual COMSOL models used to model the physical behavior of the device are shown in the COMSOL implementation section. We utilized a 3D domain that encompasses the volume within which all of the heating occurs—one that surrounds a significant volume around the probe tip and that extends outside of the area covered by the external sensor (a.k.a. the dispersive grounding electrode). This choice in domain size helps us simplify calculations as well as to reduce thermal and electrical flux at the sides of the model to zero. The sensor itself can be reduced to a boundary, and—since the device is symmetric—the domain size can be split symmetrically to reduce computation time.

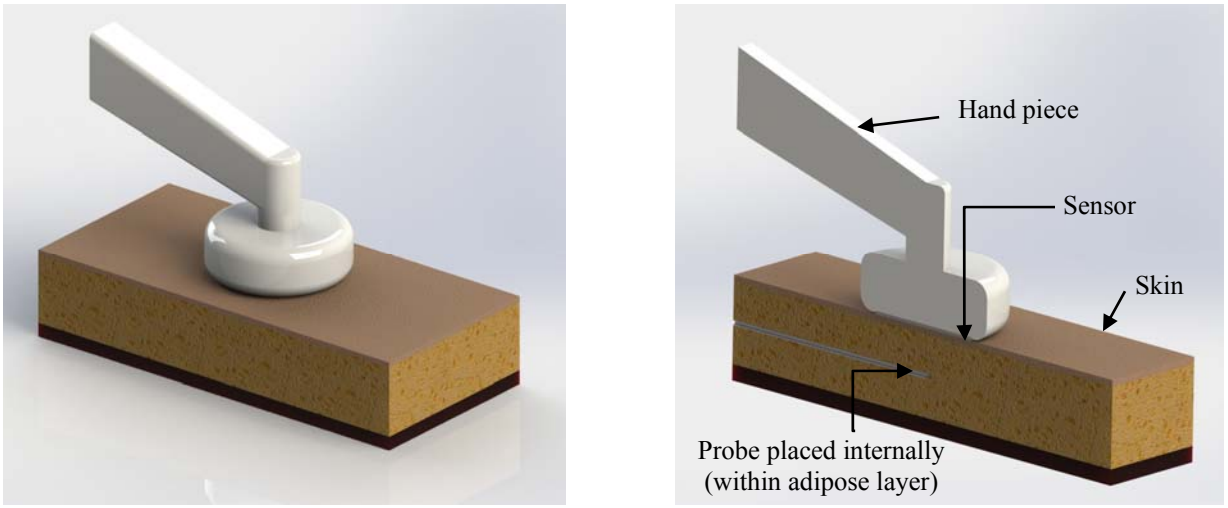


(a) (b)

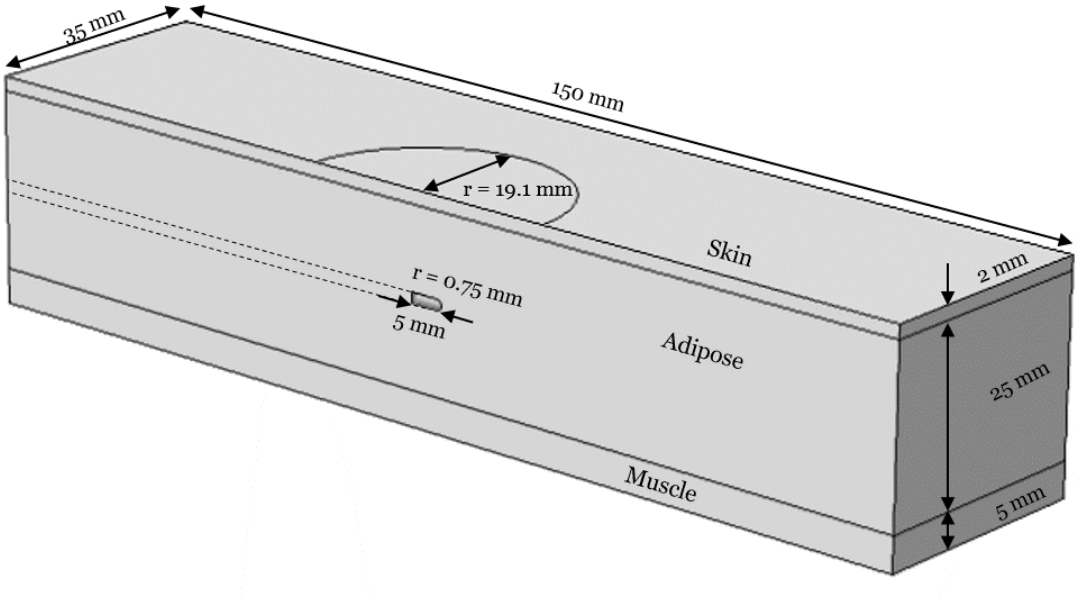


(c)

**Figure 2. 3D CAD Drawings and Schematic**

A 3D rendering of the BodyTite device to aid in conceptualizing the positioning of the various components during application. (a) External view of the device positioned during operation. (b) Cross-section of a device during typical operation. (c) A side view of the 3D model shows the associated skin, fat, and muscle thicknesses chosen for the computational model. Internal probe and external sensor dimensions are also provided.

## VI. RESULTS & DISCUSSION

Our model aimed to replicate the RFAL procedure and maximize the total volume of fat aspirated by optimizing the power and speed of operation. From the clinical studies and BodyTite Images, we extrapolated the dimensions into a CAD model shown in Figure 2 (a). The dimensions of the CAD model were implemented into a proportional 3D geometry in COMSOL with a skin, adipose, and muscle layer as shown in Figure 2 (c). Furthermore, we assume the model to be symmetric about the y-z plane in the middle as shown in Figure 2 (b), and implemented this as a symmetry physics in COMSOL.

### *Model of the Stationary Device*

The model was first implemented in COMSOL with a fixed 3D geometry and probe geometry. The heat equation was coupled to a joule heating physics that used surface voltages to drive heating. We made a quasi-static potential assumption that radiofrequency behaves like a DC voltage potential. The voltage on the probe was set in proportional to the output power of the RFAL device. Furthermore, the voltage of the sensor was set to 0V, acting as the ground. The voltage profiles at 0.001s and at 5s were computed and shown in Figure 3. We found that the gradient behavior of voltage does not change with absolute magnitude of the voltage or time. This step allows us to verify that the voltage behavior of the heat source would not change in the moving probe model.

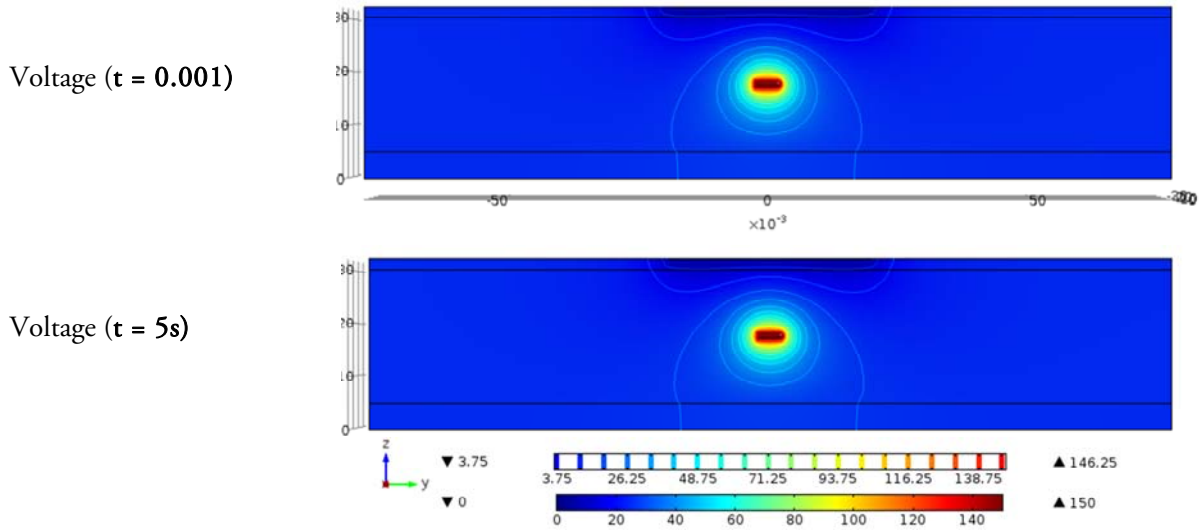


**Figure 3. Verification of constant voltage gradient**

The voltage gradient (in volts) between very early times, shortly after the device is first switched on, and at later times remains constant throughout the model simulation. Here, the voltage gradient compared between 0.001 seconds and at 5 seconds from the start of the model shows no change. This verifies that, as we expected, the electric field applied remained constant throughout the time range modeled.

*Verification of Heat Source Term in Moving Device*

In order to further verify that the moving model behaved according to the physical situation set in the static model (Figure 3) and in the wave function used to describe its motion, we plotted the heat source term within the moving model (Figure 4). This heat source term encompasses all the joule heating physics necessary to describe the RF heating, and is the basis for our moving model. We ran and visualized the simulation with very small time steps in order to avoid discrepancies, and found that the heat source does in fact behave the way we expected and moves smoothly according to the way we described mathematically.

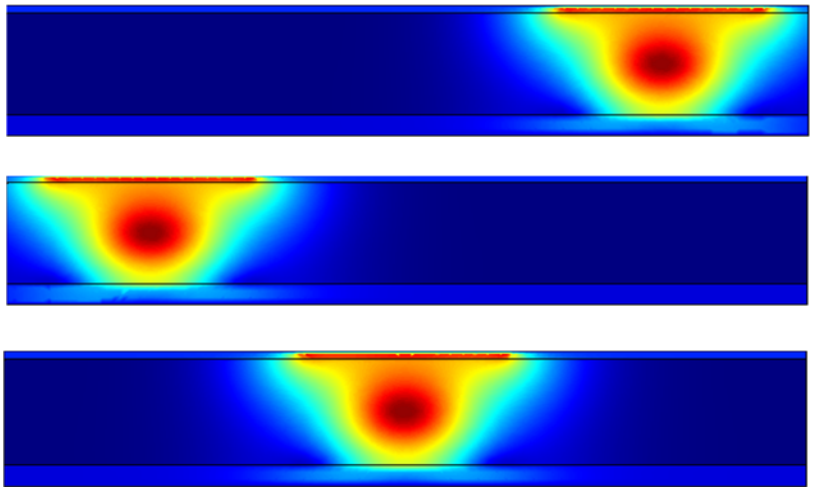

**Figure 4. Verification of the Heat Source term in the moving model**
Static images of the heat source (in terms of $W/m^3$), ranging from lowest (blue) to highest (red) heating, were taken at different time points in the model cross section during the probe movement to verify that the heat source term used in the moving model behaved realistically. The heat source term displayed the behavior that we expected in both heating behavior, with most of the heating at the probe (center) and between the probe and sensor, and movement, moving exactly the way we described mathematically.

*Model of the Moving Device*

Having successfully implemented a static model, we extended the model such that the geometry was able to accommodate the probe movement across the adipose layer. This was a more realistic representation of the clinical procedure, where the clinician moves the device to through a predetermined section of the body. The inclusion of movement to the model better describes the temperature distribution profile as observed in the clinical setting. The obtained temperature profiles were then used to calculate the volume of fat aspirated.

The geometry was altered to extend the domain and include a greater volume of skin, fat and muscle. From there, we implemented a moving heat source for both the sensor and the inside probe to simulate a moving device. The moving heat source was defined by the joule heating heat source distribution of the static model. A waveform of a triangle was selected to model a constant velocity probe moving back and

forth from the two extremes of the domain. Based on the clinical data, a velocity of 4 cm/s was chosen. An example of the resulting temperature distribution is shown in Figure 5.

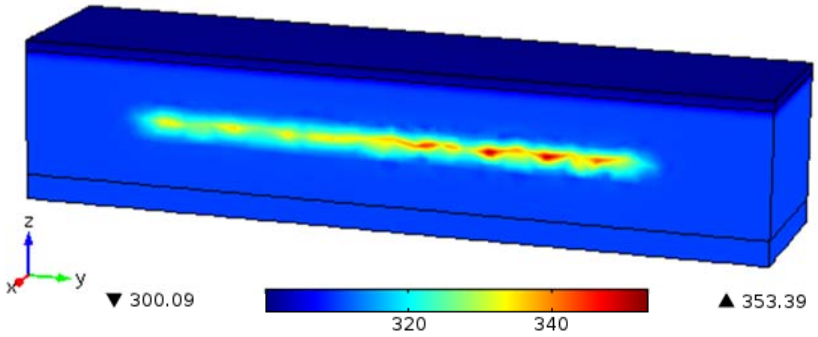


**Figure 5. Temperature Distribution of the Moving Model at t = 5s.**
The results of the moving model show a temperature distribution ranging from T = 300.09 K to T = 353.39 K, with the temperature of the skin remaining seemingly unchanged

The final parameters of the model were updated to include metabolic heat generation, convection between the skin and air, as well as blood perfusion before proceeding to sensitivity analysis and validation. The isothermal contours were plotted to show the volume of the domain that had reached at least 316 K, the melting temperature of fat, as shown in Figure 6. The volume of nodes that reach 316 K was integrated the cumulative volume of fat aspirated to validate the model. At the final time of five seconds, the volume aspirated was calculated to be 0.81455 mL for half the model (due to symmetry). We doubled this value to get a volume of 1.6291 mL of fat aspirated in five seconds of treatment time.

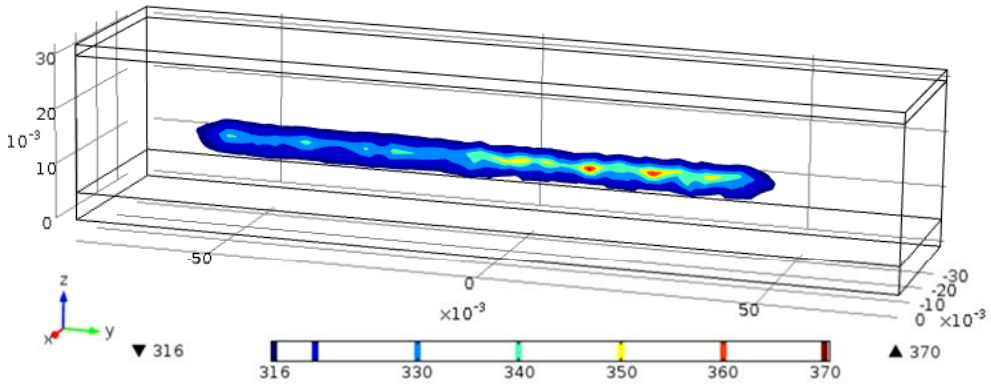


**Figure 6. Contour maps for temperatures T=316K to T=370K**
The contour regions show the volume of fat that has reached melting temperature. Due to symmetry, this volume was doubled and extrapolated to 60 minutes to compare to clinical values of fat aspiration volumes.

*Accuracy Check*

Initial verifications were performed on the material properties by an extensive literature survey, and an average of reported values were used as inputs to our system; the same is reported in table 4 in the appendices. Our decision to use a 3D symmetric schematic representation yielded us a realistic comparison to the clinical reported conditions. This was further confirmed through our validation process. The methodology adopted in our project to perform our model validation is illustrated in Figure 5.

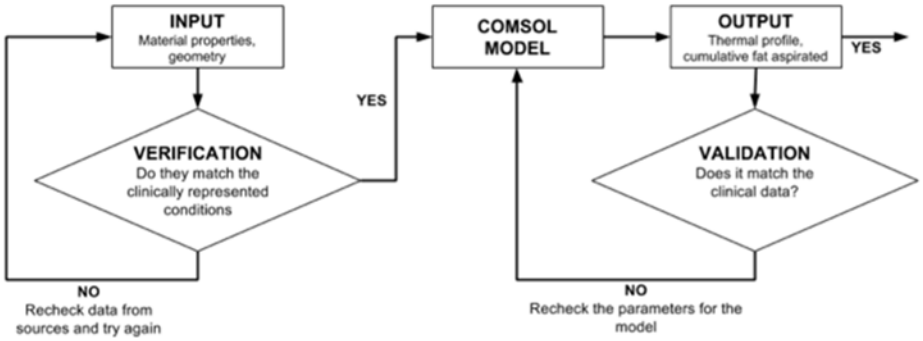


**Figure 7. Validation process used in our model**
The flowchart represents the process of system validation used to ensure the accuracy of our computational data.

In order to validate our model results, we decided to compare the cumulative volumes of fat aspirated from our model to those reported in the clinical papers **[4]**. Cumulative fat aspiration volumes were determined by performing volume integration over the adipose domain in COMSOL for different operating powers of the device. The integration was used to determine the volumes of fat that reached temperatures of 316K (43°C) or greater, which is indicative of the quantity of the adipose tissue having reached the melting point. To enable our computational results to be validated against the clinical data, we scaled our results from the five seconds obtained through our model to hour long extrapolated values, as shown in figure 9. We were able to conclude that our results fit well with the clinical reported values, thereby confirming the accuracy of our COMSOL model.

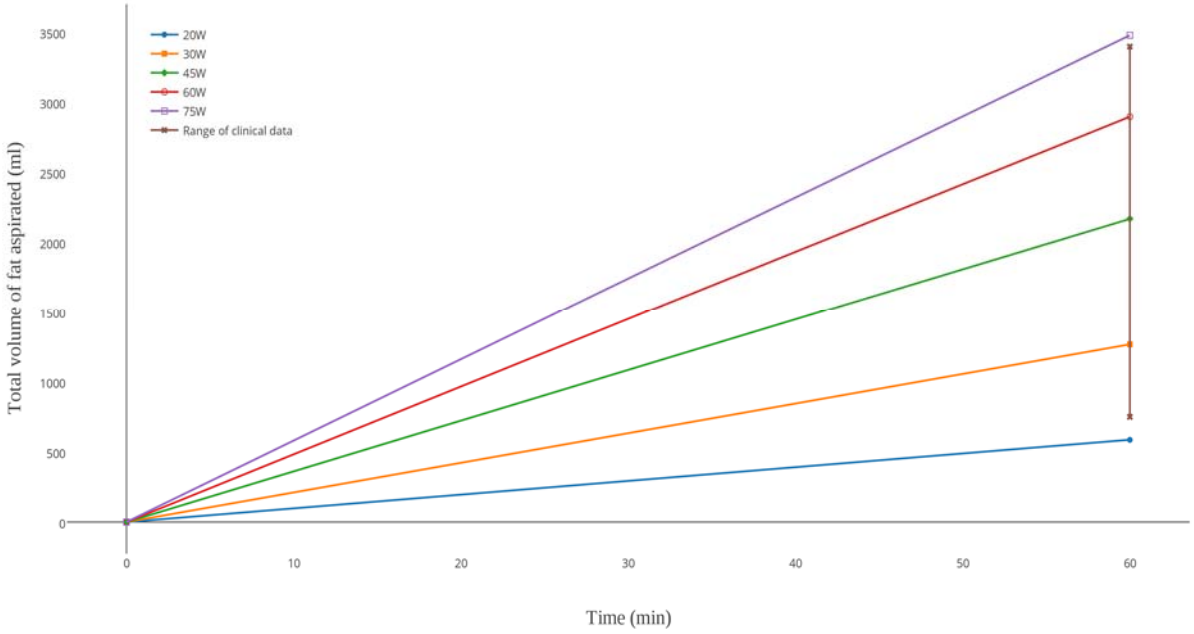


**Figure 8. Cumulative fat aspiration volumes**

The graph represents the fat aspirated as a function of time for different input powers. The vertical line is representative of the range of total volumes aspirated clinically and indicative that our data lies in within the accepted clinical norms.

*Sensitivity Analysis and Optimization*

The sensitivity analysis of our model tested the effect of varying material properties and model parameters in order to determine the uncertainty of our computational solution. There exists uncertainty within the individual material properties of our model due to the fact that many of these values, including thermal conductivity, specific heat, and density, are experimentally determined by different researchers, biological materials are inhomogeneous, and properties typically vary from person to person.

The Tissues Properties Database from the ITIS Foundation **[5]** lists materials properties of the skin, adipose, and muscle along with their corresponding standard deviation, minimum and maximum values for density, specific heat, thermal conductivity, and heat generation as shown in Table 1. From this data, we tested the uncertainty of our model by independently varying each of the properties by up to ± 2 standard deviations. The equation listed below was used to calculate the uncertainty of volume of fat aspiration for one and two standard deviations, accounting for approximately 95% of the distribution. Although it would have been optimal to test to three standard deviations, which would cover up to 99%, the equation listed is only valid for small variations, and thus, may not provide an accurate representation of the uncertainty for large changes.

$$\Delta V = \sqrt{(\frac{\partial V}{\partial \rho}\delta\rho)^2 + (\frac{\partial V}{\partial C_p}\delta C_p)^2 + (\frac{\partial V}{\partial k}\delta k)^2 + (\frac{\partial V}{\partial Q}\delta \dot{Q})^2} \quad (1)$$

The change in volume is calculated as the difference in volume of fat aspiration (regions exceeding 316K) at the final time of 5 seconds for the given tested property as compared to the baseline model value. Table 2 provides the values that were implemented into COMSOL to test the sensitivity and uncertainty of our model. The implemented values table shows that the majority of the values at ±2σ encompass the minimum and maximum values presented in the database, indicating that the sensitivity analysis covers a sufficiently large spread of data.

After testing various properties for the skin and muscle domains, we found no changes in volume aspiration. The most significant results, however, were obtained by testing properties of fat, and the results are shown in Table 4 with a graphical representation in Figure 9. After implementing the equation explained previously, for one standard deviation, the uncertainty of volume was found to be ±0.06271 mL, corresponding to an hour-long procedure aspiration volume of ±167.049 mL. For two standard deviations, the uncertainty of volume was found to be ±0.20811 mL for 5 seconds and extrapolated to ±554.413 mL for an hour-long procedure. Therefore we concluded that a 95% spread of the volume of fat aspiration ranges from 1615.55 – 2724.38 mL, corresponding well to the clinical data obtained.

An additional sensitivity analysis performed involved the dielectric properties of the material. These properties were obtained from the ITIS Tissue Properties Database as well; however, standard

deviations were not available for these properties. The uncertainty for the dielectric properties was determined by varying the frequency by ±10%. The liposuction device operates at 1MHz, and because the dielectric material properties are dependent on frequency, the model can be sensitive to error in the frequency of the device. Therefore, we tested how error in the device affects the corresponding dielectric properties and thus the solution of our model. Table 3 shows the range of values that were tested for electrical conductivity and the dielectric constant. This study found that there was no change in volume aspirated for these given values, indicating that our model is not sensitive to small changes in dielectric properties.

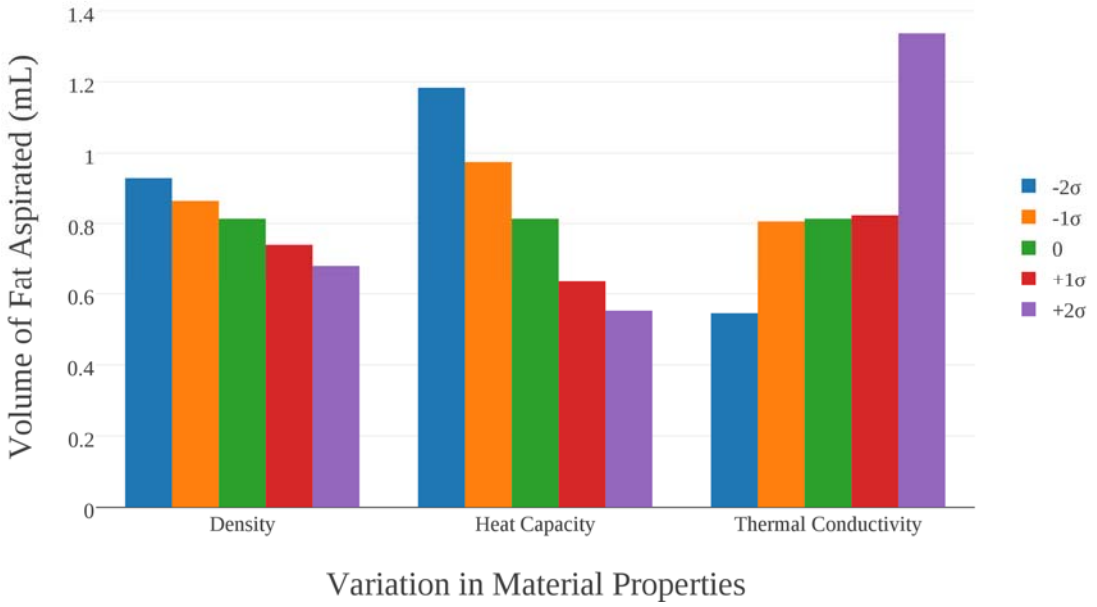


**Figure 9. Sensitivity analysis conducted on varying properties of fat**
Volume of fat aspiration decreases with increasing values of density and heat capacity of the fat domain. An opposite trend is seen for thermal conductivity, where the volume is most sensitive to a two standard deviation change.

In order to test the sensitivity of model parameters, we also investigated how power output affects the results of the computational model. Because the power output of the device can vary from 20-75 W, intervals between these two values were implemented and the results are shown in Figure 10. Consistent with our intuition, as power increases, the volume of fat aspiration also increases.

Finally, an optimization of our model was conducted by varying speed of the probe as it moves through the fat layer. We chose to test a range of speeds from 0.5 cm/s to 6 cm/s. It was hypothesized that at low speeds there would be greater amounts of fat aspirated but in a longer amount of time and the opposite would be true for high speeds. We, therefore, sought to find the most efficient speed where the rate would be maximum. The optimization was implemented by keeping the distance traveled by the

probe constant. The computation times were increased and decreased depending on the input frequency. The volume integration function was once again used to determine the volume aspirated at the final time. This volume was divided by the total computation time to determine the rate. Figure 11 shows the results, where we ultimately found the optimal speed to be 3 cm/s at a rate of aspiration of 0.1665 mL/s.

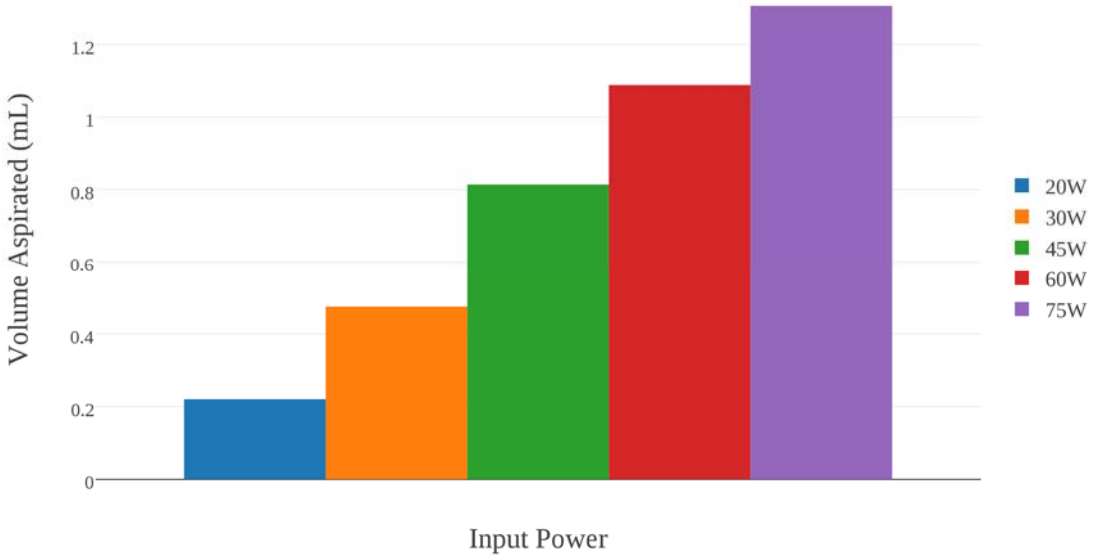


**Figure 10. Sensitivity analysis conducted on input power of the RFAL device**
Results of changing power output in the model show increasing volume of fat aspiration with increasing power.

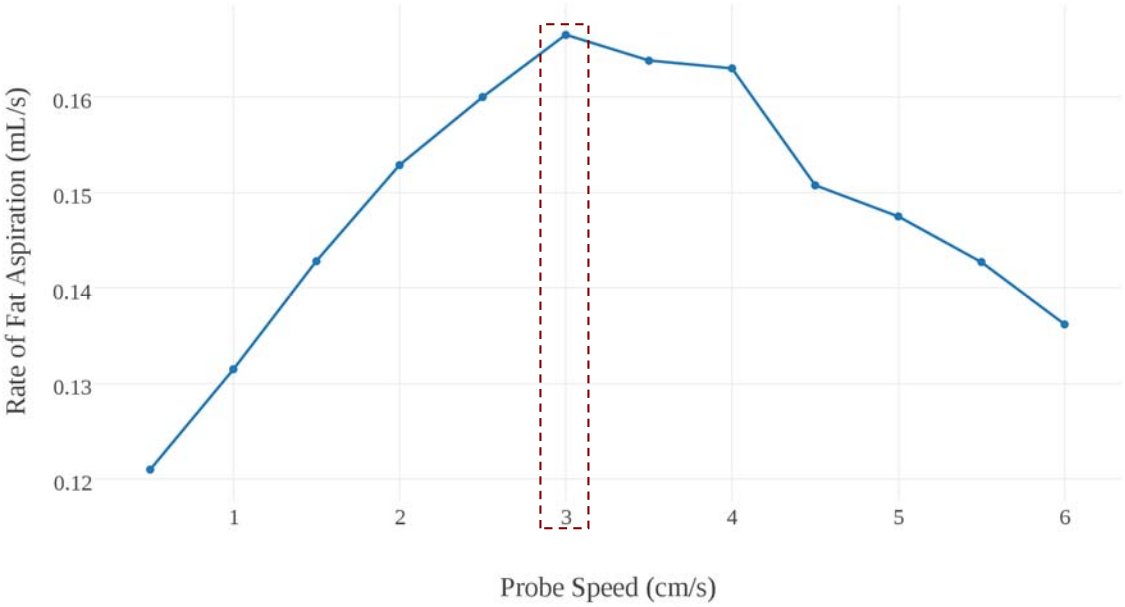


**Figure 11. Optimization of the rate of fat aspiration with probe movement speed**
Besides adjusting the power, a clinician's main control over the device during the procedure is the movement of the probe. We optimized the rate at which the device aspirates fat by running the moving model simulation at various probe velocities above and below the average velocity. The results showed that the fat aspiration could be maximized if the probe speed is controlled carefully—in this case, when the probe moves at a constant **3 cm/s.**

### *Future Work & Recommendations*

With the demonstrated potential for deriving information about the RFAL procedure and of the underlying physical situation, the current model provides a strong basis for future improvements. Further iterations using higher-order computing resources and time could account for more complexities in the real situation. These include, but are not limited to, the temperature-dependent behavior of the skin, fat, and muscle biomaterials as well as personalizing model parameters to a desired demographic and individual patients. In terms of the properties that depend on temperature, more research would need to be done in order to find comprehensive studies on those parameters that have modeled them as functions of temperature, which then can be incorporated as functions within COMSOL. In terms of personalization, although most of the biomaterial properties, such as heat capacity and electrical conductivity, cannot be realistically measured and accounted for each individual person, the geometric properties of each patient can be much more easily determined. The average thickness of the fat layer of each patient, in the location of interest (abdomen, neck, face, etc.), plays an important role in personalizing the procedure; the probe should be handled more carefully for thinner fat layers, and the power and probe velocity should be set accordingly for various thicknesses. A practical solution would be to update the design of the user interface to account for measurements of the probe velocity, or possibly to include a mechanism that adjusts the movement of the probe according to individual patient data. Overall, such considerations ensure that researchers and clinicians can optimize fat aspiration while maintaining a high standard of patient safety.

### *Acknowledgements*

We would like to take this humble little space to thank Professor Ashim Datta for his immense patience, insight, and guidance throughout the course; Alex Warning for endless knowledge of COMSOL and his unequivocal and undying sense of duty to our class; and last, but certainly not least, Dr. Nathans-Kelly for her much-needed perspective of the writing and presentation of this project, as well as her refreshing sense of humor and positivity.

## REFERENCES


[1] R. A. Weiss, 'Noninvasive radio frequency for skin tightening and body contouring', *Semin Cutan Med Surg*, vol. 32, no. 1, pp. 9–17, Mar. 2013.

[2] Surgery.org, 'News Releases - Statistics, Surveys & Trends - ASAPS Press Center - The American Society for Aesthetic Plastic Surgery Reports Americans Spent Largest Amount on Cosmetic Surgery Since The Great Recession of 2008', 2015. [Online]. Available: http://www.surgery.org/media/news-releases/the-american-society-for-aesthetic-plastic-surgery-reports-americans-spent-largest-amount-on-cosmetic-surger. [Accessed: 22- Feb- 2015].

[3] G. Blugerman, M. D., D. Schavelzon, R. Stephen, M. Sandhoffer, P. Lisborg, A. Rusciani, M. Divaris, and M. Kreindel, 'Radio-Frequency Assisted Liposuction (RFAL)', in *Advanced Techniques in Liposuction and Fat Transfer*, N. Serdev, Ed. InTech, 2011.

[4] Hurwitz and D. Smith, 'Treatment of Overweight Patients by Radiofrequency-Assisted Liposuction (RFAL) for Aesthetic Reshaping and Skin Tightening', *Aesthetic Plastic Surgery*, vol. 36, no. 1, pp. 62–71, Feb. 2012.

[5] Itis.ethz.ch, 'tissue properties database | EM material parameters | thermal material parameters | tissue material parameters | dielectric parameters | material properties | SEMCAD | Sim4Life | virtual population » IT'IS Foundation', 2015. [Online]. Available: http://www.itis.ethz.ch/virtual-population/tissue-properties/overview/. [Accessed: 25- Feb- 2015].

[6] Physics.info, 'Density - The Physics Hypertextbook', 2015. [Online]. Available: http://physics.info/density/. [Accessed: 25- Feb- 2015].

[7] M. Farvid, T. Ng, D. Chan, P. Barrett and G. Watts, 'Association of adiponectin and resistin with adipose tissue compartments, insulin resistance and dyslipidaemia', *Diabetes Obes Metab*, vol. 7, no. 4, pp. 406-413, 2005.

[8] K. Méndez J, 'Density and composition of mammalian muscle', *Metabolism*, no. 9, pp. 184-188, 1960.

[9] Itis.ethz.ch, 'tissue properties database | EM material parameters | thermal material parameters | tissue material parameters | dielectric parameters | material properties | SEMCAD | Sim4Life | virtual population » IT'IS Foundation', 2015. [Online]. Available: http://www.itis.ethz.ch/itis-for-health/tissue-properties/database/density/. [Accessed: 25- Feb- 2015].

[10] Itis.ethz.ch, 'tissue properties database | EM material parameters | thermal material parameters | tissue material parameters | dielectric parameters | material properties | SEMCAD | Sim4Life | virtual population » IT'IS Foundation', 2015. [Online]. Available: http://www.itis.ethz.ch/itis-for-health/tissue-properties/database/heat-capacity/. [Accessed: 07- May- 2015].

[11] A. Schitzer and R. Eberhart, 'Heat Transfer in Medicine and Biology', *New York: Plenum Press*, vol. 1, pp. 411-418, 1985

[12] Engineeringtoolbox.com, 'Air Properties', 2015. [Online]. Available: http://www.engineeringtoolbox.com/air-properties-d_156.html. [Accessed: 25- Feb- 2015].

[13] Itis.ethz.ch, 'tissue properties database | EM material parameters | thermal material parameters | tissue material parameters | dielectric parameters | material properties | SEMCAD | Sim4Life | virtual population » IT'IS Foundation', 2015. [Online]. Available: http://www.itis.ethz.ch/itis-for-health/tissue-properties/database/dielectric-properties/. [Accessed: 25- Feb- 2015].

[14] Itis.ethz.ch, 'tissue properties database | EM material parameters | thermal material parameters | tissue material parameters | dielectric parameters | material properties | SEMCAD | Sim4Life | virtual population » IT'IS Foundation', 2015. [Online]. Available: http://www.itis.ethz.ch/itis-for-health/tissue-properties/database/heat-generation-rate/. [Accessed: 25- Feb- 2015].

# APPENDIX

*Boundary and Initial Conditions*

The boundaries of the model are described in the table below (listed spatially from the top to the bottom of the domain) and hold for all geometric iterations of the model introduced in Figure 2. The initial temperature within the fat and muscle domains is at normative body temperature, and there is a maximum allowed threshold temperature that the system should not surpass. The main boundaries here are that of the probe (which emits the constant radiofrequency field) and that of the sensor/dispersive electrode (which grounds the radiofrequency field, having a voltage of 0). There is a small amount of convection at the skin surface, but one that is almost negligible in comparison to the other heating factors, assuming that there is minimal air flow in the operating room. Because the device is symmetrical, the COMSOL models were divided along a line of symmetry in order to reduce computation time. Initially, all domains, having zero electric field potential, were at a voltage of 0 before the device is turned on.

**Table 1: Boundary conditions of the simplified 3D BodyTite RFAL model**

| BOUNDARY | Initial Condition | Boundary Condition |
|---|---|---|
| *Top, skin/sensor* | T = 27°C | V = 0 |
| *Top, skin/air* | T = 27°C | Convection, h = 4.5 W/(m$^2$·K) |
| *Sides* | T = 37°C | dT/dx = 0 (semi-infinite) |
| *Symmetrical* | T = 37°C | dT/dx = 0 (semi-infinite) |
| *Probe/Cannula surface* | T = 37°C | V = 100 V |
| *Bottom* | T = 37°C | dT/dy= 0 (semi-infinite) |

*Governing Equations*

The relevant governing equations used within the model must describe transient, diffusive heating, as well as the heat generated from the absorption of electromagnetic energy within each 3D domain (i.e. tissue layer). The RF energy radiates solely from the tip of the probe, and the radiofrequency absorption can be described by equations derived from electromagnetics at relevant points within the domain. Biological factors such as metabolic heat generation and heat loss from blood flow are smaller in comparison, but are relevant and can be described by experimental values, though the blood flow heat loss can also be described by a simplified convective equation. Although convective heat loss at the skin surface is nearly negligible, it can also be described if necessary.

Heat Transfer in Tissue - Bioheat equation (3D):

Individually in fat, skin, and muscle layers (with respective parameters & coefficients), the bioheat equation summarizes transient heat transfer due to conduction, metabolic heat generation ($Q_m$), blood perfusion heat loss, and heat absorbed due to RF energy ($Q_{RF}$).

$$\rho C_p \frac{\partial T}{\partial t} = \underbrace{k\left(\frac{\partial^2 T}{\partial x^2} + \frac{\partial^2 T}{\partial y^2} + \frac{\partial^2 T}{\partial x^2}\right)}_{\text{conduction}} \underbrace{- \rho_b C_{p,b} V_b^{\dot{v}} (T_a - T)}_{\text{blood perfusion}} + Q_m + Q_{RF} \tag{1.1}$$

where,

$$Q_{RF} = \frac{1}{2}\sigma|\nabla V|^2 = \pi f \epsilon_0 \epsilon''_{eff}|E|^2 \approx \sigma|\nabla V|^2 = JE \tag{1.2}$$

describes the RF energy absorbed in the tissue as a function of the input frequency of the device and the electric field at a certain distance away from the source, derived from Gauss' laws from electromagnetics. the effective dielectric loss is a function of the tissue's frequency-dependent electrical properties.

$$\nabla \cdot (\sigma \nabla V) = 0 \tag{1.3}$$

(Gauss' Law for electric flux)

&

$$\epsilon''_{eff} \approx \frac{\sigma}{\epsilon_0 \omega} = \frac{\sigma}{\epsilon_0 2\pi f} \tag{1.4}$$

is the effective dielectric loss, i.e. energy dissipation

Convective Heat Transfer between Skin and Air

Only at top boundary, in addition to the bio-heat equation, there is convection due to the air (though very small).

$$Q_{conv} = h_{skin,air}A(T_{air} - T_{skin}) \quad (1.5)$$

*Sensitivity Analysis Tables*

**Table 2: Material properties with the standard deviation**

| *Domain* | *Description* | *Average* | *St. Dev.* | *Min* | *Max* |
|---|---|---|---|---|---|
| Skin | Density [kg/m$^3$] | 1109 | 14 | 1100 | 1125 |
| | Specific Heat [kJ/(kg·K)] | 3.391 | 0.233 | 3.15 | 3.662 |
| | Thermal Conductivity [W/(m·K)] | 0.37 | 0.06 | 0.32 | 0.5 |
| | Heat Generation [W/kg] | 1.65 | 0.57 | 0.76 | 2.7 |
| Adipose | Density [kg/m$^3$] | 911 | 53 | 812 | 961 |
| | Specific Heat [kJ/(kg·K)] | 2.348 | 0.372 | 1.806 | 2.973 |
| | Thermal Conductivity [W/(m·K)] | 0.21 | 0.02 | 0.18 | 0.24 |
| | Heat Generation [W/kg] | 0.51 | 0.2 | 0.31 | 0.98 |
| Muscle | Density [kg/m$^3$] | 1090 | 52 | 1041 | 1178 |
| | Specific Heat [kJ/(kg·K)] | 3.421 | 0.46 | 2.624 | 3.799 |
| | Thermal Conductivity [W/(m·K)] | 0.49 | 0.04 | 0.42 | 0.56 |
| | Heat Generation [W/kg] | 0.91 | 0.32 | 0.46 | 2.32 |

**Table 3: Implemented material property values.**

| *Domain* | *Property* | *-2σ* | *-1σ* | *0* | *+1σ* | *+2σ* |
|---|---|---|---|---|---|---|
| Skin | Density [kg/m$^3$] | 1081 | 1095 | 1109 | 1123 | 1137 |
| | Specific Heat [kJ/(kg·K)] | 2.925 | 3.158 | 3.391 | 3.624 | 3.857 |
| | Thermal Conductivity [W/(m·K)] | 0.25 | 0.31 | 0.37 | 0.43 | 0.49 |
| | Heat Generation [W/kg] | 0.51 | 1.08 | 1.65 | 2.22 | 2.79 |
| Adipose | Density [kg/m$^3$] | 805 | 858 | 911 | 964 | 1017 |
| | Specific Heat [kJ/(kg·K)] | 1.604 | 1.976 | 2.348 | 2.72 | 3.092 |
| | Thermal Conductivity [W/(m·K)] | 0.17 | 0.19 | 0.21 | 0.23 | 0.25 |
| | Heat Generation [W/kg] | 0.11 | 0.31 | 0.51 | 0.71 | 0.91 |
| Muscle | Density [kg/m$^3$] | 986 | 1038 | 1090 | 1142 | 1194 |
| | Specific Heat [kJ/(kg·K)] | 2.501 | 2.961 | 3.421 | 3.881 | 4.341 |
| | Thermal Conductivity [W/(m·K)] | 0.41 | 0.45 | 0.49 | 0.53 | 0.57 |
| | Heat Generation [W/kg] | 0.27 | 0.59 | 0.91 | 1.23 | 1.55 |

**Table 4: Frequency-dependent dielectric properties**

| *Domain* | *Property* | *Frequency (MHz)* | | | | |
|---|---|---|---|---|---|---|
| | | *0.90* | *0.95* | *1* | *1.05* | *1.10* |
| Skin | Dielectric Constant | 1000 | 998 | 991 | 984 | 977 |
| | Electrical Conductivity | 0.0112 | 0.0122 | 0.0132 | 0.0143 | 0.0154 |
| Adipose | Dielectric Constant | 51.5 | 51.2 | 50.8 | 50.5 | 50.2 |
| | Electrical Conductivity | 0.044 | 0.044 | 0.0441 | 0.0441 | 0.0441 |
| Muscle | Dielectric Constant | 2060 | 1940 | 1840 | 1740 | 1650 |
| | Electrical Conductivity | 0.495 | 0.499 | 0.503 | 0.506 | 0.51 |

**Table 5: Volume of Fat Aspirated (mL) for varying fat properties**

| | *-2σ* | *-1σ* | *0* | *+1σ* | *+2σ* |
|---|---|---|---|---|---|
| Thermal Conductivity | 0.545117 | 0.806756 | 0.814551 | 0.824298 | 1.33731 |
| Density | 0.92942 | 0.864951 | 0.814551 | 0.74078 | 0.680983 |
| Specific Heat | 1.18335 | 0.974818 | 0.814551 | 0.635118 | 0.552221 |

## *Material Properties*

**Table 6: All relevant material properties**
Properties were compiled throughout various online databases, most of which compile statistical values from multiple studies.

| | *PROPERTY* | *VALUE* | *SOURCE* |
|---|---|---|---|
| $\rho_{skin}$ | *Density skin* | 1109 kg/m$^3$ | [7] |
| $\rho_{adipose}$ | *Density adipose* | 911 kg/m$^3$ | [8] |
| $\rho_{muscle}$ | *Density muscle* | 1090 kg/m$^3$ | [9] |
| $C_{p,skin}$ | *Specific heat skin* | 3.391 kJ/(kg·K) | [11] |
| $C_{p,adipose}$ | *Specific heat adipose* | 2.348 kJ/(kg·K) | [11] |
| $C_{p,muscle}$ | *Specific heat muscle* | 3.421 kJ/(kg·K) | [11] |
| $k_{skin}$ | *Thermal conductivity skin* | 0.37 W/(m·K) | [12] |
| $k_{adipose}$ | *Thermal conductivity adipose* | 0.21 W/(m·K) | [12] |
| $k_{muscle}$ | *Thermal conductivity muscle* | 0.49 W/(m·K) | [12] |
| $\epsilon_{0,skin}$ | *Dielectric constant skin* | 991 at 1MHz | [14] |
| $\epsilon_{0,adipose}$ | *Dielectric constant adipose* | 50.8 at 1MHz | [14] |
| $\epsilon_{0,muscle}$ | *Dielectric constant muscle* | 1840 at 1MHz | [14] |
| $\sigma_{skin}$ | *Electrical conductivity skin* | 0.0132 S/m at 1MHz | [14] |
| $\sigma_{adipose}$ | *Electrical conductivity adipose* | 0.0441 S/m at 1MHz | [14] |
| $\sigma_{muscle}$ | *Electrical conductivity muscle* | 0.503 S/m at 1MHz | [14] |
| $q_{gen,\ skin}$ | *Heat gen. skin* | 1.65 W/kg | [15] |
| $q_{gen,\ adipose}$ | *Heat gen. adipose* | 0.51 W/kg | [15] |
| $q_{gen,\ muscle}$ | *Heat gen. muscle* | 0.91 W/kg | [15] |
| $\rho_{blood}$ | *Density blood* | 1050 kg/m$^3$ | [10] |
| $C_{p,blood}$ | *Specific heat blood* | 3.617 kJ/(kg·K) | [11] |
| $k_{blood}$ | *Thermal conductivity blood* | 0.52 W/(m·K) | [12] |
| $V_{blood}$ | *Blood volumetric flow rate (skin)* | 6.67E-6 to 46.7E-6 m$^3$/(m$^3$·s) | [13] |
| $C_{p,air}$ | *Specific heat air* | 1.005 kJ/(kg·K) (20$^o$C, 1atm) | [14] |
| $h_{skin,\ air}$ | *Heat transfer coefficient between skin and air* | 4.5 W/(m$^2$·K) | [6] |

*Mesh Convergence*

The heating behavior between the probe tip and the sensor, especially near the probe tip, is expected to have the largest changes in voltage and the most intense heating. The behavior that we are most interested in is during the period that the radiofrequency wave front penetrates the layers above the probe and becomes grounded at the sensor. This is when the field contours surrounding the probe tip transforms from a purely cylindrical-like shape into a more parabolic one, directed upward toward the sensor. Modeling this behavior is pertinent to accurately representing the heating profile observed clinically and therefore obtaining mesh convergence is contingent on an accurate temperature at a point chosen close to the probe tip, between the center of the probe tip and that of the sensor (x=0,y=0,z=0.02m). Based on the mesh convergence plot, as shown in figure 12, convergence of values begins at an element size of 25,452 and begins stabilizing at 56, 626 elements. We chose to distribute the meshing such that the fat domain had a great mesh compared to the skin domain while still retaining the 56,626 elements in total, as shown in figure 13.

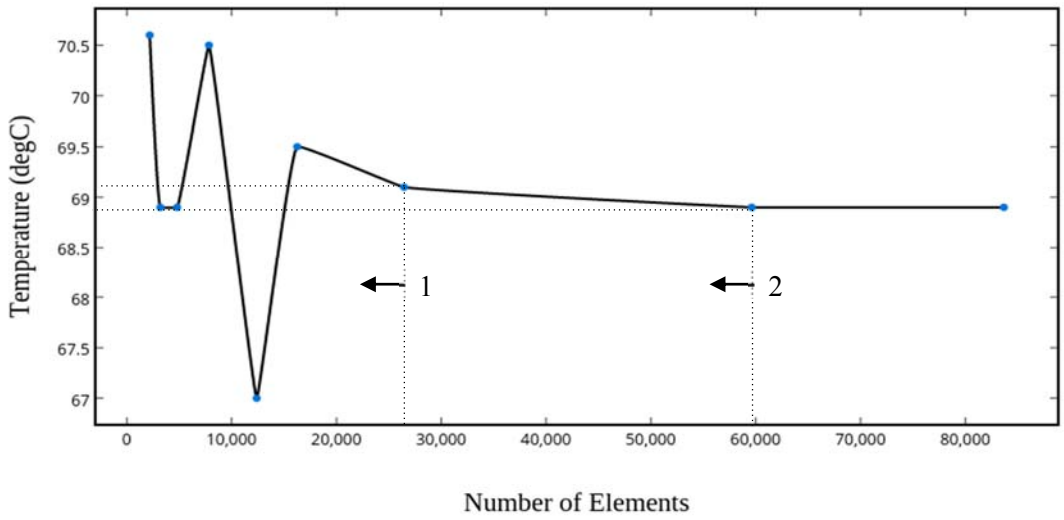


**Figure 12. Mesh convergence**

A plot comprising temperature ranging in 67-70.5°C with element sizes from 2182 to 83,672 was obtained and convergence was found to occur at an element size of 25,452 (indicated by the dotted line 1). The element size that we chose to use for our model was 56,625 (indicated by the dotted line 2)

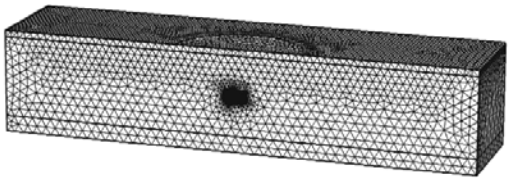

**Figure 13. Meshing used in our model**

Mesh convergence was performed at interface between the electric fields generated by the probe and the sensor, which represents the point of maximum temperature flux within the adipose layer. A visual representation of the positioning of this point in relation with the model is shown. The skin layer contains a lower meshing element size than the adipose layer, because of the smaller changes in temperature occurring in this region.